Assessing the thermal efficiency of energy tunnels using numerical analysis and the Taguchi statistical approach.

Oluwaseun Ogunleye[1]; Rao Martand Singh[2]; Francesco Cecinato[3]

[1]*Department of Civil and Environmental Engineering, Faculty of Engineering and Physical Sciences, University of Surrey, Guildford, GU2 7XH, UK.*

[2]*Department of Civil & Environmental Engineering, Norwegian University of Science & Technology (NTNU), Trondheim 7034, Norway.*

[3] *Dipartimento di Scienze della Terra "Ardito Desio", Università degli Studi di Milano, via Mangiagalli 34, 20133 Milan,* Italy.

Corresponding author's email: o.ogunleye@surrey.ac.uk

Abstract

The use of ground source heat pump systems (GSHPs) with tunnels (so-called energy tunnels) to provide space heating and cooling is one of the latest concepts that has recently raised research interest, but has not yet been commercially established. This study represents a first attempt to investigate the influence of design parameters on the energy efficiency of a GSHP using an underground tunnel as the energy geostructure. Seven important design parameters, namely absorber fluid diffusivity, concrete diffusivity, pipe thermal conductivity, pipe diameter, length of pipe, pipe spacing and absorber pipe location were considered. The influence of these design parameters on the tunnel thermal efficiency was studied by using an experimentally validated 3-D numerical model and then deploying the Taguchi method to efficiently explore parameters space. The results show that concrete diffusivity and pipe total length are the most influential parameters, followed by the pipe location and diameter, while spacing was found to be the least influential factor. Hence the overall thermal output of an energy tunnel depends largely on the available area for heat exchange and the thermal properties of the tunnel lining. Results also show that within the range of pipe diameter considered, using a larger pipe diameter in energy tunnels is more efficient from the point of view of thermal output and pump power requirements. These results can be used as thermal efficiency optimisation guidance for both researchers and practitioners.

Keywords: Energy tunnel, geothermal, thermal efficiency, numerical modelling, Taguchi method.

1. Introduction

Shallow geothermal energy (SGE) is commonly extracted for building heating/cooling purposes and as a source of warm water [1], ground source heat pumps (GSHPs) are usually used to extract SGE. They have emerged in recent years as a viable and sustainable system for the heating and cooling of buildings compared to other heat pump systems [2]. However, to be able to rely on GSHPs as long-term sustainable systems, comprehensive research is needed to understand the role of ground conditions and design parameters on the thermal efficiency of these systems [3].

SGE installations can be open-loop or closed-loop. In open-loop systems, the transfer of thermal energy is achieved directly from the ground by pumping water from underground aquifers, extracting/rejecting heat by means of a heat pump and then transferring the water back to the ground [4]. In closed-loop systems, the so-called primary circuit consists of a series of ground heat exchangers (GHE) while the secondary circuit is represented by the heating/cooling system located in the designated building. A working fluid is circulated within the GHE to exchange heat between the ground and the building via a heat pump. Open loops are characterised by higher efficiency relative to closed loops, but the latter can bring about advantages in terms of avoiding typical operational problems such as the risk of clogging resulting from mineral precipitation [5].

Closed-loop systems can be installed in so-called energy geostructures, upon burying heat absorber pipes within an underground structure, usually made of reinforced concrete [6]. The most common energy geostructures are foundation piles, diaphragm walls and tunnels [7]. In underground tunnels **(Fig. 1)**, heat absorber pipes are typically embedded inside the lining segments, which are in contact with the ground on their outer side and air on the inner side. Tunnels equipped with GHE are also known as energy tunnels and are the focus of this research. An important advantage of energy tunnels over the other aforementioned structural heat exchangers is the very large soil-structure contact surface potentially available for heat exchange.

Some of the most important ground parameters affecting the geothermal potential of energy tunnels are soil thermal properties, groundwater flow rate, and underground air temperature [8]; while some important design parameters of energy tunnels are: absorber fluid thermal properties, concrete lining thermal properties, length of pipe and pipe spacing [9]. The influence of the above-mentioned ground parameters on the thermal performance of energy tunnels has already been investigated, showing that the ground thermal conductivity, groundwater velocity and tunnel temperature all affect the energy tunnel's thermal output [3].

Since ground parameters are site-specific, and little can be done to alter or improve them, the focus of an energy efficiency analysis is always on the design parameters. The effect of design parameters on other energy geostructures (pile and diaphragm wall) has been investigated in the literature (e.g. [6], [10], [11] [12]). The analysis carried out on pile heat exchangers showed that the number of pipes and the pipe length are the dominant parameters [6]. In diaphragm walls, the pipe spacing was found to be most influential factor followed by the concrete thermal properties [10].

In energy tunnels, the geometry and boundary conditions are substantially different from other GHEs (i.e. piles and walls). Understanding the relative impact of design parameters on the thermal output of geothermal energy tunnels is important for the thermal design of these systems. This aspect has hardly ever been explored in the literature. This paper presents a first attempt to investigate the effect of design parameters on the thermal output of energy tunnels through a parametric study, to provide optimisation guidance for engineers and researchers. This research is conducted using numerical and Taguchi statistical analysis.

The paper is structured as follows: A background study on previous work carried out to study the effect of design parameters on GSHPs is presented in section 2, followed by section 3 which entails the methodology used in this study, describing the validation and implementation of a 3D numerical model. Section 4 describes the model application and the choice of parameter range, while Section 5 focusses on the parametric analysis using the Taguchi method. Results from the parametric study and further analysis are discussed in Section 6. Finally, the conclusion of this study is presented in Section 7.

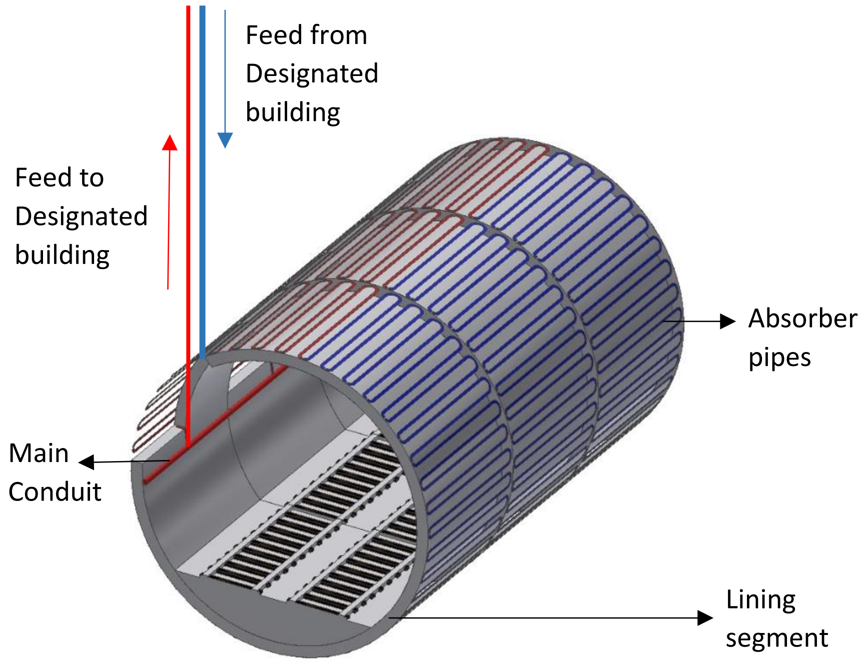

Fig. 1. Schematic of an example energy tunnel

2. Background

This section focusses on previous work carried out on GSHP systems to improve and optimise important design parameters.

2.1. Pipe configuration and pipe length

The effect of absorber pipe configuration (Transverse, longitudinal and slinky) and location on the energy tunnel output has been investigated [13, 14], the transverse configurations having resulted in higher thermal efficiency, even though the total length of heat exchange pipe in slinky configuration increased three-fold. The results obtained also show higher thermal output when absorber pipes are located closer to the inside of the tunnel. Sani, Singh [15] also investigated the effect of pipe-pipe thermal interaction on a GHE and concluded that both the number of loops and pipe location influence the system's thermal efficiency.

When thermal interference between absorber pipes is controlled, increasing the total area available for the heat exchange process increases the thermal output in the majority of GHE systems. This trend has been analysed by various research studies (e.g. [6] [10] [13] [14]). Ultimately the required pipe length for a project is normally dictated by the heating or cooling demand; however, managing pressure drop is always crucial due to the corresponding pump power requirement [16].

2.2. Pipe thermal conductivity

The thermal conductivity of HDPE pipes used in a BHE can be increased from 0.4 to 0.7 W/m k by adding carbon nanoparticles [17]. This increase in conductivity reduces thermal resistance, which in turn can reduce the required borehole length by 23 percent in a coaxial GHE [17]. A study conducted by [18] involved the use of HDPE and aluminium wires composite to enhance the thermal conductivity of the pipes. The aluminium wires were embedded and equally spaced within the pipe. Depending on the numbers of wire fillers used, the thermal conductivity increased between 25 and 150 percent. The use of stainless steel pipes in GHE has also been investigated [19]. Since the thermal conductivity of steel is 40 times that of commonly used HDPE, results show an improvement in the system's performance. However, the study highlighted that there are potential corrosion problems and the associated cost analysis has not been included in the study. Another example is that of manufacturer IPL, who was able to improve the thermal conductivity of HDPE by 75 percent (0.7 W/m k) by mixing additives to the polymer resin used to extrude the pipe [20]. Subsequent simulations carried out on a single U-bend shows a reduction of 24% in borehole thermal resistance resulting in a shorter required borehole length [20].

2.3. Pipe diameter

The choice of pipe diameter for a particular operation depends on multiple factors: pump power requirements, the available area for heat exchange, heating or cooling demand and the required radius of curvature [21]. The choice of pipe diameter thus becomes an important parameter in the design of GSHPs. For example, in a GSHP system using shallow building foundation as the energy geo-structure, the heat exchange rate was found higher for smaller diameter pipe compared to larger diameters for the same velocity and total length of pipe [22]. On the other hand, using experimental and numerical analysis, Luo, Zhao [23] concluded that the thermal efficiency of a U- type GHE increased using a large pipe diameter (32 mm) compared to a small diameter (25 mm) for energy piles; however, it should be noted that the flow rate used for the 32 mm (1.85 L/s) was higher than the 25 mm (1.57 L/s). Contrarily, varying the diameter between 20 mm, 25 mm, and 32 mm did not have a significant effect on the thermal performance in a study on horizontal GHEs conducted by [24].

2.4. Fluid velocity

The mass flow rate in a pipe is related to the magnitude of the fluid velocity, hence the turbulence in the pipe. An increase in velocity increases the turbulence which in turn increases the heat transfer rate [25]. The choice of fluid velocity was found to be among the critical factors affecting the efficiency of a GHE [26], [27]. The mass flow rate influences the rate of transfer of thermal energy and the mean energy transfer increases as the velocity increases [28]. The optimum velocity range recommended by Zhou, Lv [29] for vertical ground heat exchangers using u-shaped single 32 mm, double 25 mm and 32 mm pipes are 0.4–0.6, 0.4–0.5, 0.3–0.4 m/s respectively. The thermal resistance of a vertical U-tube GHE decreases with an increase in fluid velocity, implying an increase in the heat exchange rate [30]. The heat exchange rate was found to increase when the fluid velocity was increased from 0.3 m/s to 0.4 m/s; however, the rate of increase of heat exchanged reduced with further increase in fluid velocity i.e. from 0.4 m/s to 0.9 m/s [30]. An optimum value of 0.6 m/s was recommended, this value takes account of the efficiency and pumps power. Also, it is important to note that the increase of fluid velocity could become inconsequential in the thermal performance of GHEs once turbulence is reached [6] [10].

2.5. Absorber fluid thermal properties

Water with antifreeze is normally deployed as the working fluid in closed-loop GSHPs in cold climatic conditions. Sodium chloride, calcium chloride and ethylene glycol solutions are the most commonly used antifreeze solutions in GSHP applications [9]. The addition of antifreeze ensures the system can work below 0℃. However, operating costs reduce with the use of pure water without antifreeze, due to the increase in thermal conductivity, so in mild climates, pure water should be used [31]. The use of antifreeze in operations where the heat pump would invariably work below freezing allows for a larger temperature difference between the circulating fluid and the surrounding medium. The use of water in these cases is impossible [32]. Recently, to improve the thermal properties of heat transfer fluid, so-called nanofluids are sometimes used as the working fluid, where solid nanoparticles with high thermal conductivity are added to the base fluid (water) [12]. The effect of using Al_2O_3/water nanofluids on the efficiency of vertical GSHPs, due to the improved thermal conductivity and viscosity was assessed by [33], resulting in a reduction of 1.3 percent bore length of the GHE compared to using pure water.

2.6. Concrete thermal properties

Tunnel linings are primarily designed to withstand structural loads imposed by the surrounding ground and self-weight. Depending on local availability, different aggregate mixes are used [34]. As a result, different concrete thermo-physical properties are obtained. **Table 1** illustrates the concrete lining thermal properties for different regions/tunnels described in the literature. The table includes a concrete mix with enhanced thermal conductivity (3.09 W/m k) developed for use in tunnel linings in Korea [14]. In an effort to increase the thermal conductivity it can be seen below that a relatively higher density (3640 kg/m^3) is needed. This should be taken into account in structural calculations.

Table 1. Thermal properties for different tunnel lining.

Properties	Republic of Korea (Korean Patent, 2003) [14]	Linchang Tunnel China [35]	Metro Torino line Italy [8]	Crossrail UK [36]
Thermal Conductivity (W/m K)	3.09	1.85	2.3	1.33
Heat capacity (J/kg K)	840	970		750
Density (kg/m^3)	3640	2400		2500
Volumetric Heat capacity (MJ/m3/K)			2.19	

3. Numerical Modelling

In this study, to investigate the effect of the design parameters illustrated in Section 2, a previously developed 3-D numerical model [7] and validated against experimental tests is employed. The model was developed using the finite element software ABAQUS complemented by bespoke user subroutines. The main heat transfer processes considered in the numerical model are:

- The conduction heat transfer between the tunnel lining and the surrounding soil,
- The convective heat transfer between the working fluid and the pipe wall,
- The convective heat transfer between the tunnel air and the tunnel wall (set as a boundary condition [7]).

Due to the small thickness of the pipe wall, the heat capacity of the pipe wall is negligible relative to the absorber fluid, concrete lining and soil heat capacities; hence the transient heat transfer in the pipe wall was not considered in the model.

Other forms of heat transfer, such as thermal radiation in the soil and advection in the presence of groundwater, have not been considered in the model. While the former is negligible except in a very coarse soil [37], the latter is relevant to cases of flowing groundwater in medium-high permeability soil or fractured rock. Hence, the present model is relevant to GHEs installed in fine-grained (low permeability) soil, unfractured rock and granular soil in the absence of flowing groundwater. In any case, the model could be easily extended to include groundwater advection. Outlined below are the model's governing equations.

Conduction heat transfer in the ground and concrete is governed by Fourier's law [38], it is usually expressed as shown in **Eq. (1):**

$$q'' = -k\frac{\partial T}{\partial n}n \tag{1}$$

where q'' is the heat flux in the direction of a unit vector n, T is the temperature, k is the thermal conductivity. The transient heat equation is thus written as [38]:

$$\frac{\partial^2 T}{\partial x^2} + \frac{\partial^2 T}{\partial y^2} + \frac{\partial^2 T}{\partial z^2} + \frac{\dot{q}}{k} = \frac{1}{\alpha}\frac{\partial T}{\partial t} \tag{2}$$

where t is the time and α is the thermal diffusivity and $\dot{q}$ is the internal heat generation rate. The convective heat transfer between the tunnel air and the tunnel lining is related by [39]:

$$-k_L\frac{\partial T}{\partial n} = h[T_L - T_\infty] \tag{3}$$

where h is the convective heat transfer coefficient between the tunnel air and the tunnel lining, T_L is the temperature of the tunnel lining surface, T_∞ is the air temperature, k_L is the thermal conductivity of the tunnel lining. Also, the convective heat transfer between the absorber pipe and the tunnel lining are related by:

$$-k_L\frac{\partial T}{\partial n} = h_{eq}\left[T_l - T_f\right] \tag{4}$$

where T_f is the working fluid temperature, T_l is the temperature of the tunnel lining on the outside surface of the pipe and h_{eq} described in **Eq. (5)** is the equivalent convective heat transfer coefficient [39]. This was introduced in the model by combining the thermal resistance of the pipe wall and the thermal resistance for convection due to the movement of the working fluid.

$$h_{eq} = \left[\frac{D_{out}}{2k_{pipe}}\ln\left(\frac{D_{out}}{D_{in}}\right) + \frac{D_{out}}{D_{in}h}\right]^{-1} \tag{5}$$

where k_{pipe} is the thermal conductivity of the pipe, h is the convective heat transfer coefficient of the working fluid, D_{out} and D_{in} are the outer and inner pipe diameters respectively.

The heat extracted is calculated using the thermal energy equation, expressed as:

$$Q = \dot{m}C_p(T_{out} - T_{in}) \tag{6}$$

Where Q is the heat extracted, $\dot{m}$ is the mass flow rate in the pipe, C_p is specific heat capacity while T_{out} and T_{in} are the outlet and inlet temperature respectively.

3.1. Numerical model implementation

The heat transfer problem was simulated in ABAQUS as previously mentioned, the convective heat transfer due to the fluid flow in the pipes was implemented using user-defined subroutines FILM and URDFIL [7]. The pipes were represented in 1-D as lines of nodes in the model; however, the appropriate (3-D) pipe lateral surface areas associated with each node were represented in the subroutine. The FILM subroutine was used to define the heat transfer coefficient and associated sink temperatures, in order to calculate the temperature of subsequent nodes. Moreover, subroutine URDFIL was used to access the code result file to obtain the heat flux from previous nodes. The model only considered one tunnel ring in the simulation.

The numerical model was validated against field data gathered from Linchang energy tunnel [40]. The validation was performed by comparing the measured outlet fluid temperature, showing good agreement between numerical and experimental data [7]. Additional validations were also carried out in this study to further assess the suitability of the model in reproducing the heat transfer phenomena in energy tunnels, as described below.

3.2. Model Validation - Using the obtained Outlet fluid temperature from a laboratory-scale energy tunnel

3.2.1. Geometry and discretisation

The numerical validation using the result of a laboratory experiment [41] is discussed in this sub-section. The domain size is 1 m x 1 m x 0.36 m **(Fig. 2)**. The size of the geometry corresponds to the soil boundary of the experimental model. DC3D8 hexahedral heat transfer 8-node linear heat transfer elements were used in this validation exercise. The DC3D8 element was assigned to the geometry, with the optimum number of nodes and elements of 100225 and 92280 respectively. The results (steady-state outlet temperature attained) converged at 100225 element size by carrying out a mesh sensitivity analysis, hence a solution independent of the mesh size was achieved.

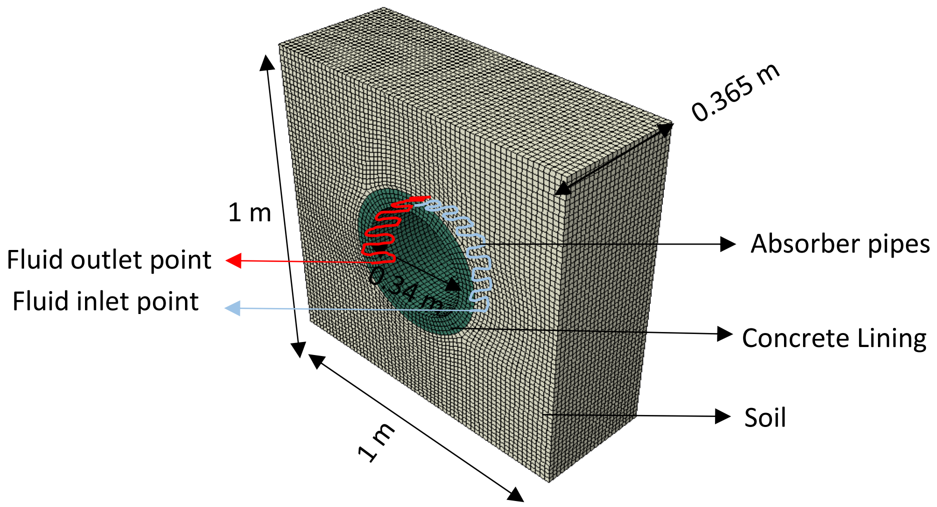

Fig. 2. Geometry and dimensions for model validation (Laboratory experiment)

3.2.2. Initial and boundary conditions

The initial temperature for the whole domain was set to 17.5°C, this corresponds to the initial surrounding soil temperature of the experiment. The heat transfer coefficient was estimated by using the correlation proposed by [42], taking into account the effect of thermal conductivity, air velocity and relative humidity. Using the laboratory measured values (1.6 W/ m k, 3 m/s and 80% respectively), the heat transfer coefficient was estimated as 15 W/m^{2}k. This value is consistent with the value obtained using the correlation given in [43]. During the experiment the tunnel exhibited an average air temperature of 16.9°C, with a marginal fluctuation that was captured in the simulations by defining a periodic tunnel air temperature. The water inlet temperature was given a value of 4°C.

3.2.3. Material properties

The material parameters and boundary conditions for this validation are presented in **Table 2**. The tunnel diameter is 34 cm, the lining has a thickness of 5.5 cm. The absorber pipe spacing is 4.8 cm with a total length of 9.6 m.

Table 2. Test data from the laboratory experiment

Parameter	Value
The inner diameter of the tunnel	34 cm
Lining thickness	5.5 cm
Pipe spacing	4.8 cm
Pipe Length	9.6 m
Absorber pipe outer diameter and wall thickness	6.35mm, 1.59 mm
Heat transfer coefficient inside the tunnel	15 W/m^{2}K
Inlet fluid temperature	4°C
Fluid velocity	0.7 m/s
Tunnel air temperature	Varied (average 16.9°C)
Surrounding soil temperature	17.5°C

Material Properties:

	Thermal conductivity (W/m K)	Density (kg/m^3)	Specific heat (J/kg K)	Dynamic viscosity
Circulating fluid	0.56	980	4200	1.5×10^{-3} m^2/s
Concrete lining	1.6	2115	1862.88	
Surrounding soil	1.1	1414.3	798.98	

For a given fluid inlet temperature and velocity, the numerical model yields as output the corresponding outlet temperature at a given time and the temperature distributions in the soil.

The simulation time was 8 hours, enough for the outlet fluid temperature to reach a steady-state condition. The numerical results are compared to the laboratory results in terms of measured outlet fluid temperature in **Fig. 3.** Good agreement between numerical and experimental results can be obseved. Further evaluation of the results was carried out by determining the overalll root mean square error (RMSE) of the residuals (**Table 3)**. Also, **Fig. 3** shows the relative error between the laboratory data and the model as a function of time.

At the start of the simulation, a relative error of around 14% was attained, to then decrease towards the end of the simulation, when it was around 9%. This observation shows that the model becomes relatively more accurate once the operation reaches a steady state. Overall it can be observed that the model can reproduce the heating operation of an energy tunnel to an acceptable degree.

Table 3. RMSE result for the heating operation (outlet temperature).

Period	Global	0 – 2 hrs	2 – 4 hrs	4 – 8hrs
RMSE	0.6	0.68	0.38	0.66

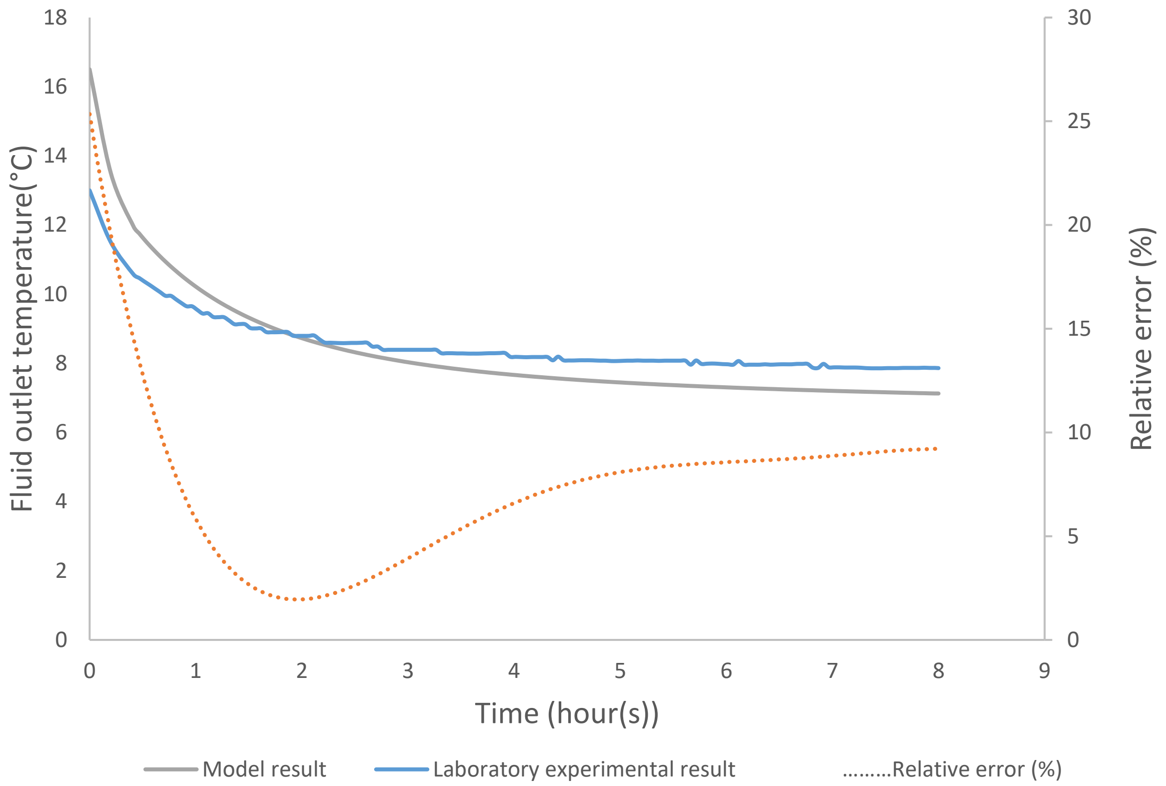

Fig. 3. Model validation against the experimental result from [41] in terms of outlet fluid temperature.

3.3. Model validation – Using the soil temperature distribution obtained from the laboratory experiment

This validation exercise was carried out to further assess the suitability of the model in predicting the soil temperature distribution in an energy tunnel. Accurate predictions of the soil temperature changes in any GSHP system is vital to estimating its true geothermal potential. Also, there are legal implications in some instances when the soil temperature perturbations due to the operation of GSHPs are not controlled [7]. The geometry, material properties and boundary conditions in this validation are the same as in section 3.2. The soil temperature results obtained from the model agreed well with the experimental results. In fact, the initial transient period (0 -2hrs) and the steady-state period (6-8) were accurately captured by the model. The temperature obtained at different time intervals from the simulation and the experiment is illustrated in **Fig. 4.** The RMSE for this simulation is plotted in **Table 4**. Overall it can be said that the model can accurately predict the soil temperature distribution due to the operation of an energy tunnel to an acceptable degree.

Table 4. RMSE results for the heating operation (soil temperature distribution).

Period	Global	2 hrs	5 hrs	8hrs
RMSE	0.35	0.35	0.41	0.28

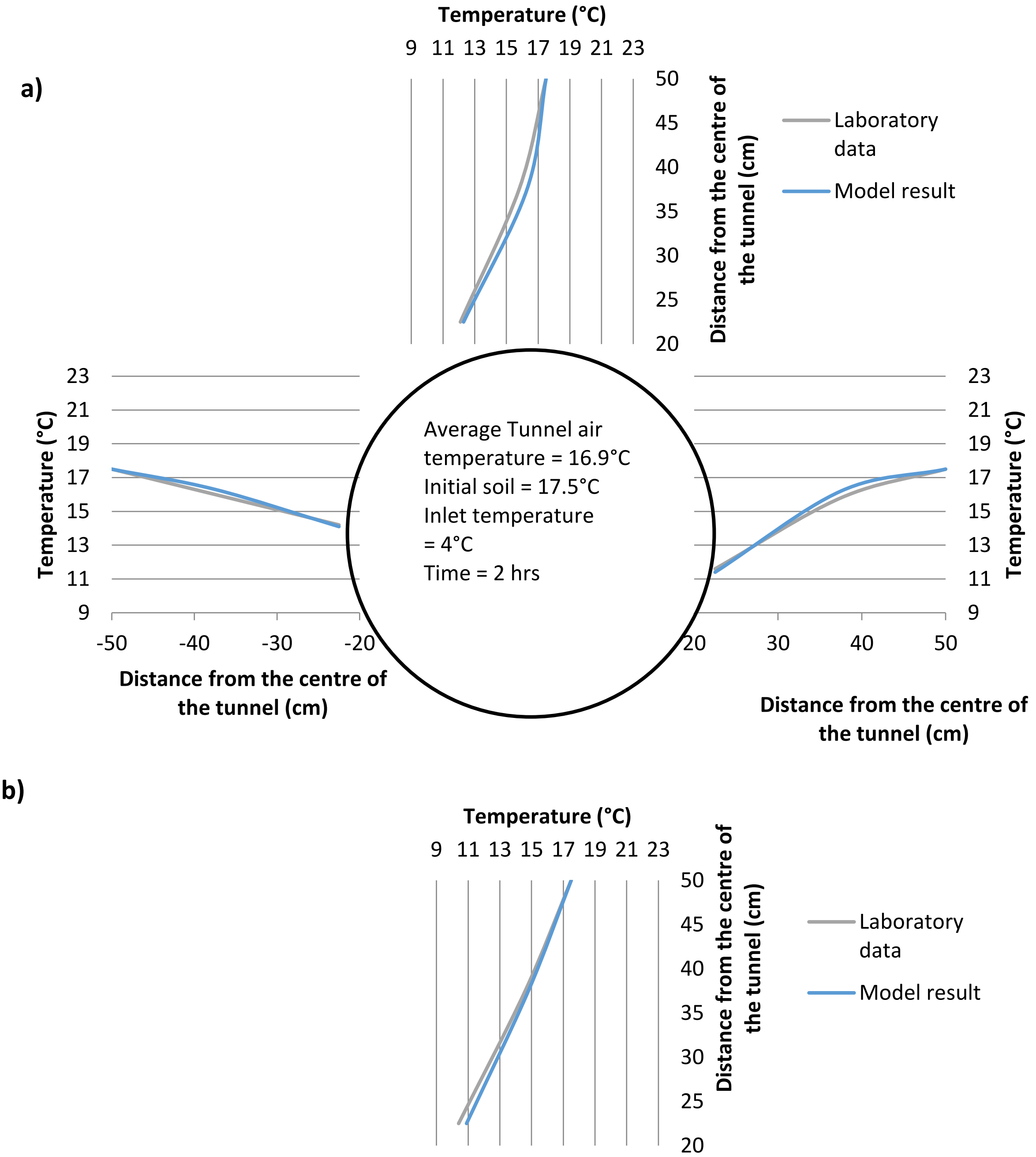

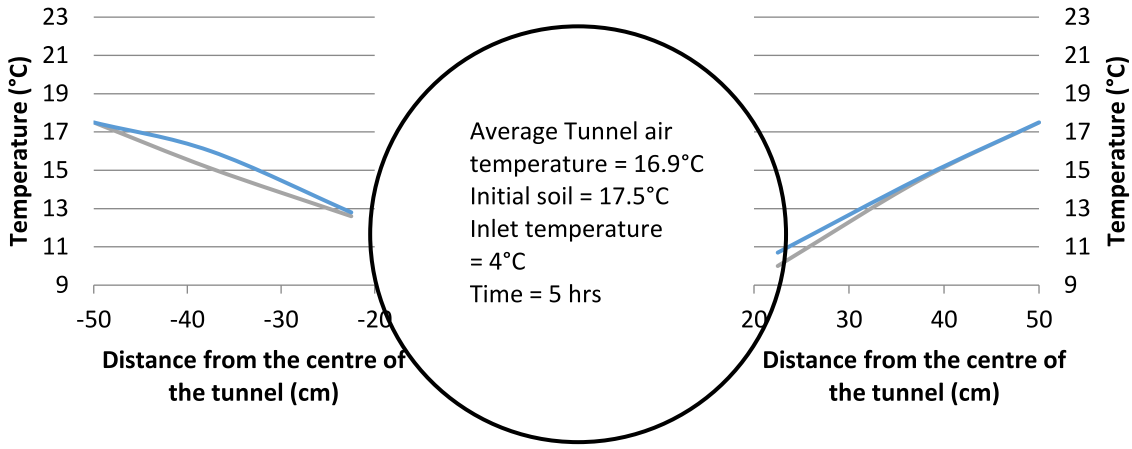

c)

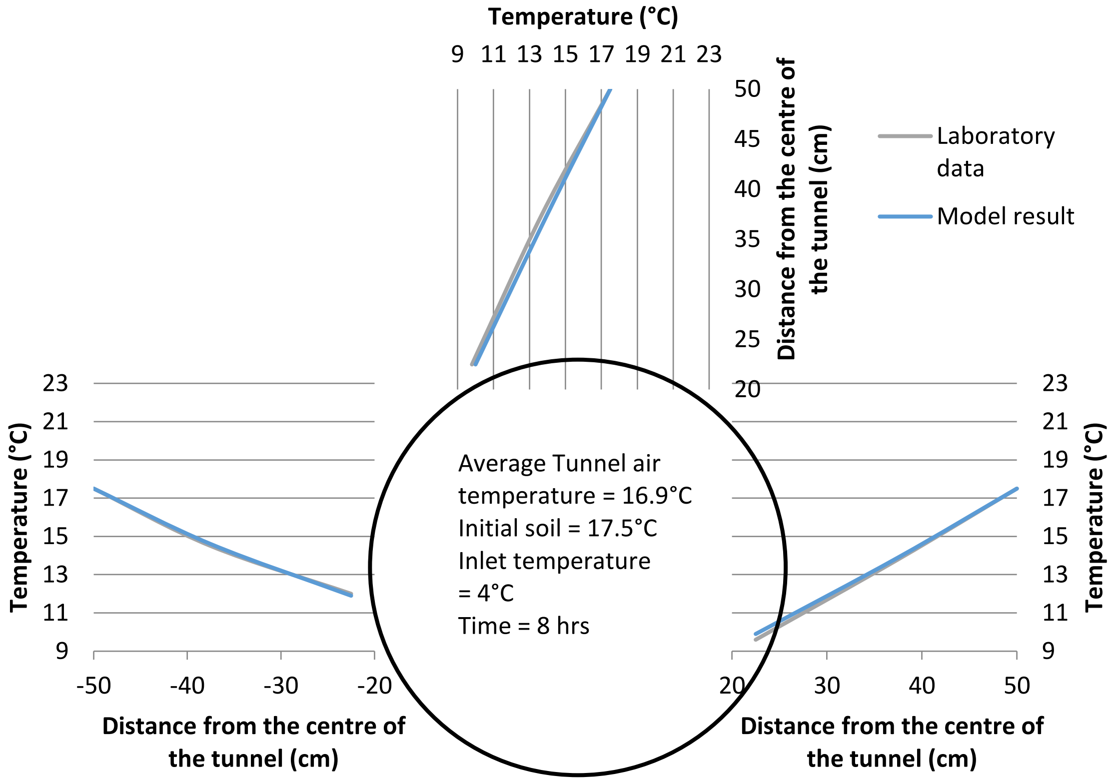

Fig. 4. Model validation with the experimental result from Laboratory model (soil temperature distribution). a) After 2 hours b) After 5 hours c) After 8 hours.

4. Model application

The model was then applied to investigate the influence of different design parameters on the thermal performance of energy tunnels. This was realised by performing several heat extraction simulations for 10 days, and varying design parameters according to a specific strategy defined via the Taguchi method described in section 5. The time of simulation can be considered large enough to explore the transient behaviour in the majority of instances, and short enough to save computational time [6]. Model parameters that are site-specific (such as ground parameters mentioned in the introduction) or cannot be altered, and those that are expected to have a comparatively small effect with their variation (based on previous studies, e.g. [6], [10], [11]), are kept constant and assigned a realistic average value based on published values. For example, the effect of fluid velocity has been shown to become inconsequential once turbulence is reached (Reynolds numbers between 4000-5000) [6], [10], hence this parameter was kept constant. The parameters considered are: absorber fluid diffusivity, concrete diffusivity, pipe thermal conductivity, pipe diameter, length of pipe, pipe spacing and absorber pipe location. These parameters were selected since they have emerged in recent literature as influential in the performance of other energy geostructures [6] [10] [11] [12] [15], as well as having received significant attention in terms of research and development [12] [20] [44] [49].

4.1. Choice of parameter range

The next task after selecting the parameters is to determine realistic ranges for them while making sure the parameters' effects do not interfere with each other [45] [46]. Considering the thermophysical properties of the absorber fluid and concrete lining, it is a common practice to focus on the thermal conductivity. However, in this study, the thermal diffusivity was used as a parameter. Diffusivity measures "the ability of a material to conduct thermal energy relative to its ability to store thermal energy" [38]. Materials with large diffusivity will respond rapidly to changes in their thermal environment, while materials with small diffusivity take longer to reach a new equilibrium condition [38]. Since heat transfer in energy tunnels takes place as a transient phenomenon, focusing on thermal diffusivity appears more realistic, and more representative of the overall thermo-physical properties of a material, compared to thermal conductivity. Moreover, diffusivity is more suitable in terms of statistical independence [47] in a Taguchi analysis.

Considering realistic ranges for absorber fluid diffusivity, the values used were taken from Ghozatloo et al. [44], who investigated heat transfer enhancement using graphene nanofluids. The addition of 0.075 percent of graphene resulted in an increase of 31.83 percent in thermal conductivity and also a 35.6 percent increase in the convective heat transfer coefficient at a concentration of 0.1 wt% relative to water. **Table 5** below shows the thermal properties achieved.

Table 5. Properties of improved nanofluids, graphene and water, adapted from [44].

	Graphene ratio % wt	**%vol**	**Density *ρ* (kg/m³)**	**Thermal Conductivity *k* (W/mK)**	**Specific heat c_p (J/kg K)**	**Thermal Diffusivity α (m²/s) (x 10⁻⁷)**	**Viscosity m (Pa s)**
Water	0	0	995.8	0.601	4179.1	1.44417	0.000891
Graphene	1	1	2200	5000	790	0.0028767	
KRG-2	0.05	0.023	1023.8	0.704	4009.4	1.71506	0.0009429

KRG-3	0.075	0.035	1038.4	0.791	3924.9	1.94081	0.0009698
KRG-4	0.1	0.048	1053.5	0.689	3840.1	1.70311	0.0009977

KRG-number - indicates the graphene nanofluids and the corresponding reference number

As regards pipe outer diameter, the typical pipe size ranges from 20 mm to 30 mm [6] [48], it should be noted that the ratio between the inner diameter and the outer diameter is kept constant at 0.82.

For pipe spacing, the limit is ultimately determined by the minimum bend radii of the HDPE pipes. In order to meet the minimum bending radii, a spacing of 20 - 30cm is typically used in energy tunnel projects [48], [36], [8].

Considering the location of the absorber pipes, assuming the tunnel segments are fabricated using the standard segmental lining manufacturing process [48], the concrete cover will not be affected whether they are tied to the top or bottom of the reinforcement layer. As a result of this, the two extremes of positioning the pipes were used in this study that is: 10 cm of radial distance from the tunnel arc measured from the inner surface of the tunnel (attached to the bottom of the cage) and 20 cm from the tunnel arc (attached to the top of the cage).

Transient heat transfer in the pipe wall was not considered in the model due to its relatively small thickness, as explained in **section 3.** Hence, thermal conductivity becomes the key thermo-physical property for the absorber pipe. This parameter typically ranges between 0.3 W/m K and 0.4 W/m K [6] [12]; however, thermally enhanced pipe have been achieved in some cases [20], [12], reporting on average a value 0.6 W/m K.

The total length of pipes is usually dictated by the thermal energy requirements and the available area for heat exchange, hence a larger diameter tunnel will increase the total length available. Depending on the geometry of the tunnel, a 50 to 80 m pipe length per lining segment (The length of segments is typically between 1.4 m and 1.6 m) has been achieved in previous projects [49] [13] [48] [50] [51].

The range of concrete diffusivity **(Table 6)** was taken from [52], the study examined the thermophysical properties of concrete with limestone aggregates and enhanced thermophysical properties of concrete by adding high conductive aggregates and metallic fibres. The range selected was 5.3 – 15.6 m^2/s with the lower value corresponding to a limestone aggregate and upper value for a conductive concrete with 8% copper fibre.

Table 6. Concrete thermal properties with highly conductive aggregate [52].

Concrete	Thermal conductivity (W/m k)	C_p (J/kg K)	Density (kg/m^3)	Thermal Diffusivity ($x10^{-7}$) (m^2/s)
Lytag (Insulative concrete)	0.5	1245	1559	2.9
Limestone	1.2	1033	2255	5.3
Quatzite +1% Cu fiber	3.6	935	2502	15.6

conductive concrete				
Quatzite +8% Cu fiber (conductive concrete)	10.7	920	2590	44.9

4.2. Numerical model settings

The geometry of a particular tunnel depends on the type of project and also the soil's thermal properties are site-specific. Due to the availability of data, the tunnel geometry and soil thermal properties were taken from the Torino metro project (Italy) as an example [8]. The distance from the centre of the tunnel to the top surface is 21.5 m and the tunnel diameter is 6.8 m with 30 cm lining thickness. The overall domain size is 43 m x 43 m x 2 m. Regarding undisturbed soil temperature, a constant value of 14˚C was considered which is a typical value in Turin as reported in the literature [50, 53]. Also, a constant value of 15 W/m^{2}K was assigned for the convective heat transfer coefficient and an average bulk air temperature of 18˚C was set at the air/lining interface [10, 35, 50]. A tunnel could be regarded as ‘cold’ or ‘hot’ depending on the difference between the internal air temperature and the ground surface temperature [7]. It is worth noting the imposed difference between the initial soil temperature and air temperature here (4˚C), this was done in order to observe the effect of absorber pipe location.

Linear hexahedral elements were used in this study and the mesh was refined closer to the absorber pipes, as represented in **Fig. 5**. Typically, the results (steady-state outlet temperature attained) converged at 184400 elements as shown in **Table 7**, hence a solution independent of the mesh size was achieved. **Table 8** highlights the main parameters that were kept constant in the simulations.

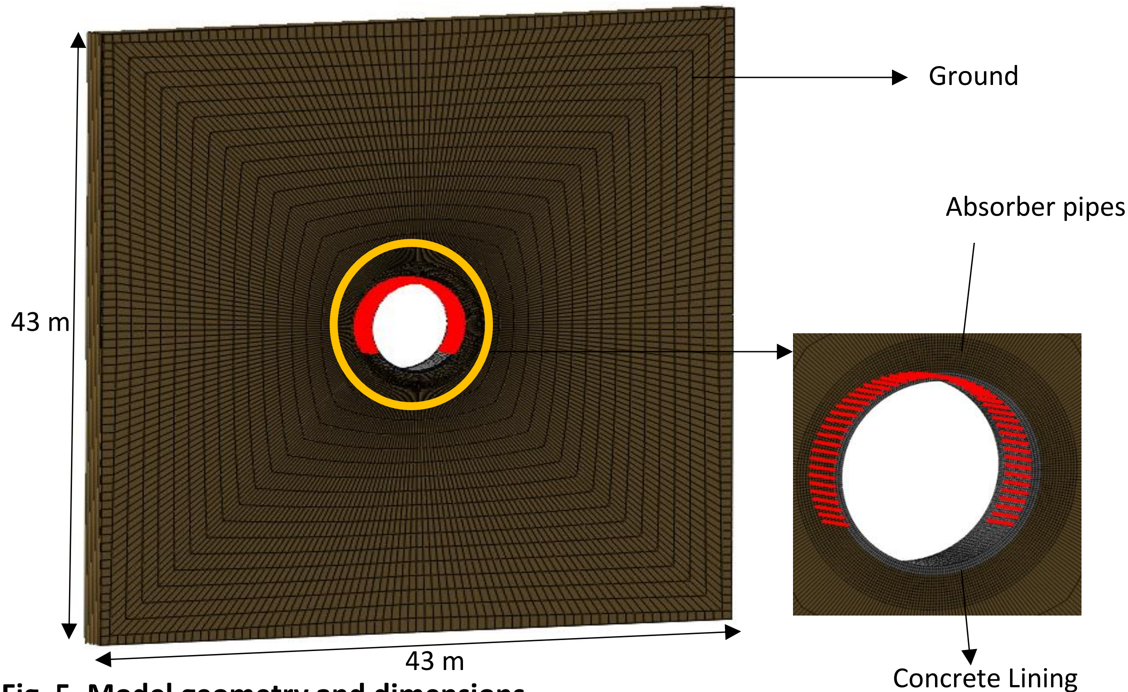

Fig. 5. Model geometry and dimensions

Table 7. Mesh refinement study

Number of elements	Steady-state outlet temperature (°C)
145008	9.227
152353	9.444
162811	9.546
184400	9.612
199562	9.613

Table 8. Constant parameters in the simulation.

Parameter		Value
Tunnel diameter		6.8 m
Tunnel thickness		300 mm
Tunnel overburden		21.5 m
Inlet fluid temperature:		4˚C
Initial soil temperature		14˚C
Heat transfer coefficient between tunnel air and lining		15 W/m^{2}K
Tunnel air temperature		18˚C
Working fluid flow velocity		0.4 m/s
	Thermal conductivity	Heat Capacity
Surrounding soil	2.8 W/m K	2.0 MJ/kg K

5. Parametric analysis using Taguchi Method

The parametric analysis was designed using the criteria of experimental design, which is a branch of engineering statistics [46]. This method involves the variation of variables in an operation, in order to observe the effect of the variation on a response variable. For the purpose of this study, the Taguchi statistical experimental design approach was deployed due to its simplicity and efficiency [6, 10, 45, 46]**.** For a parametric study involving the seven parameters discussed above, a total of eight simulations is required with the Taguchi method. Alternatively, if full factorial methods were deployed where all possible parameter combinations are considered, this would result in a large number of simulation runs, the total number of possible combinations being 7^2 =49 [10]. In order to reduce the number of needed experiments, the Taguchi method involves the formation of adequate orthogonal arrays. A Taguchi array is formed of a 2D matrix with each row of the matrix signifying the dataset of a particular experiment to be conducted while each column holds all the values of one of the variables.

The most important property of the so-called orthogonal array is that the columns are statistically independent [6]. An indication of a very influential parameter is when the outputs on one of its levels are considerably different from the results on another one of its levels [10] [46] [47]. For a particular parameter, “the levels of the other parameters occur an equal number of times for each level of the parameter, hence their effect will be cancelled out in the computation of the given parameter’s effect. The estimation of the effect of any parameter is thus accurate and reproducible [47]”.

Two levels in most cases are considered adequate to design the matrix set i.e. an upper bound and a lower bound value. For the parameter to have a quantifiable effect, the upper bound and lower bound are set to realistic extreme values. **Table 9** shows the selected parameter ranges **(see section 4.1).** For the number of parameters considered (seven) a 2 level Taguchi analysis, with *L*8 orthogonal array was deployed [47], with the resulting array shown in **Table 10**. Analyses are then carried out by running one simulation for a given set of variables. A total of 10 days of heat extraction was simulated. The exchanged power for each simulation can be calculated using **Eq. 7 :**

$$Q(t) = \dot{m}c_w|T_{wO} - T_{wi}| \tag{7}$$

where $\dot{m}$ is the mass flow rate, T_{wi} is the inlet temperature of the pipe and T_{wO} is the outlet temperature. **Table 10** also shows the response (thermal response) of each simulation in terms of heat extracted in 10 days per unit area, as

$$Q_{total} = \int_0^t Q(t)dt\,/A \tag{8}$$

with t the time and A the tunnel surface area.

Table 9. Parameter levels

Parameter	Lower bound	Upper bound	units
Fluid Diffusivity	1.44E-07	1.94E-07	m^2/s
Pipe diameter	20	30	mm
Pipe spacing	20	30	cm
Pipes thermal conductivity	0.3	0.6	W/m K
Pipe length	50	80	m
Concrete diffusivity	5.3	15.6	m^2/s
Concrete cover	10	20	cm

Table 10. Taguchi L8 othrogonal array table

run	Fluid Diffusivity (m^2/s)	Pipe diameter (mm)	Pipe spacing (cm)	Pipes Conductivity	Total length (m)	Concrete diffusivity (m^2/s)	Concrete cover (cm)	Response W/m^2

	$*10^{-7}$			(W/m K)		$*10^{-7}$		
1	1.44	20	20	0.3	50	5.3	10	22
2	1.44	20	20	0.6	80	15.6	20	53.45
3	1.44	30	30	0.3	50	15.6	20	38.08
4	1.44	30	30	0.6	80	5.3	10	46.07
5	1.44	20	30	0.3	80	5.3	20	33.34
6	1.94	20	30	0.6	50	15.6	10	41.54
7	1.94	30	20	0.3	80	15.6	10	57.75
8	1.94	30	20	0.6	50	5.3	20	20.47
C	1.94	20	30	0.6	80	15.6	10	63.14

C represents the confirmation run

6. Results and Discussion

The interpretation of the result entails carrying out a level average analysis on the thermal output obtained in order to find the parameters that are most influential [6]. The analysis consists of the following:

- Finding the average simulation result for each level of parameter
- Quantifying the effect of each parameter by finding the absolute difference between the highest and the lowest average result
- Ranking the parameters based on their effect.

The result of the Taguchi analysis is presented below in **Table 11**

Table 11. Taguchi response table (Output after 10 days, W/m^2)

	Fluid Diffusivity	**Pipe diameter**	**Pipe spacing**	**Pipe thermal conductivity**	**Total length**	**concrete diffusivity**	**Concrete cover**
max	153.107	162.3753	159.0395	161.528	190.6046	190.8221	167.3571
min	159.6035	150.3352	153.671	151.1825	122.1059	121.8884	145.3534
response	6.49652	12.04001	5.368547	10.34544	68.49871	68.93369	22.00371
Rank	6	4	7	5	2	1	3

Table 11 shows the ranking of the parameters in the last row from the most to the least influential in maximising the thermal performance, as follows: concrete diffusivity, total length, concrete cover and pipe diameter, pipe thermal conductivity, fluid diffusivity and pipe spacing. The effect of the three lowest-ranked parameters cannot be evaluated with confidence due to the statistical nature of this type of analysis [6], hence the main focus

should be put on the top 4. In addition, a confirmation run [47] was carried out (as a form of reliability check) using the upper bound parameter/optimal parameter settings. As expected, the thermal output for the confirmation run resulted in the highest output (63.14 W/m^2).

The table also shows a very small difference between the response obtained for the pipe total length and concrete diffusivity, hence for practical purposes they can be considered tied at the top of the ranking. The concrete cover and the pipe diameter were ranked third and fourth respectively, highlighting the importance of the location of the absorber pipes and the size of the heat exchanger pipes. The two least influential parameters are pipe spacing and fluid diffusivity.

The outlet fluid temperature obtained for different runs and the corresponding heat rate was plotted versus time in **Fig. 6 and Fig. 7.** It should be noted that runs with higher steady-state outlet temperature do not necessarily correspond to a higher heat rate. This can be explained from the difference in pipe diameter resulting in different mass flow rate. For example, the result of run 1 resulted in the 5th highest steady-state outlet temperature but had the lowest heat rate together with run 8.

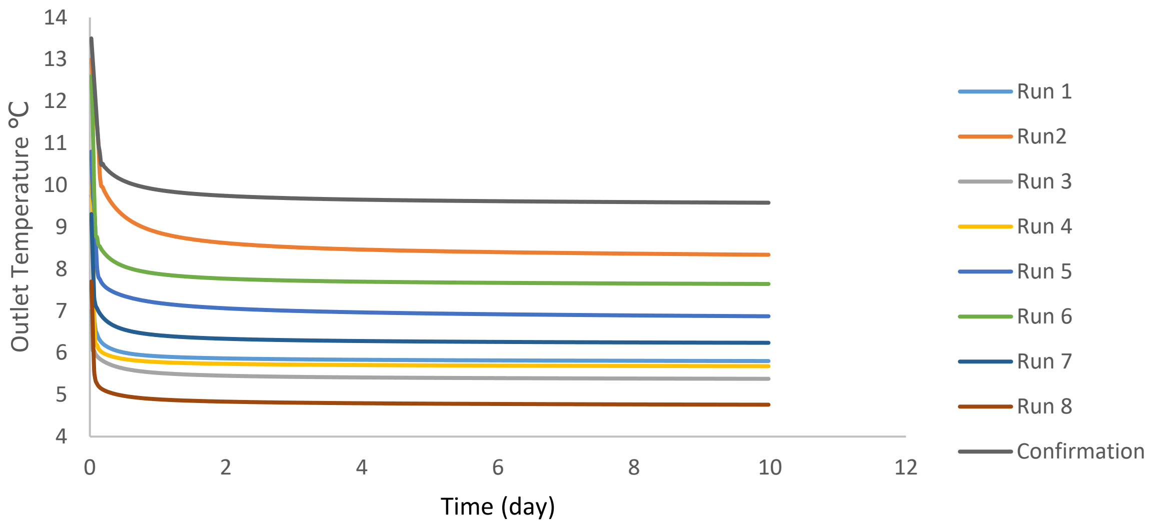

Fig. 6. Outlet fluid temperature history for all the runs

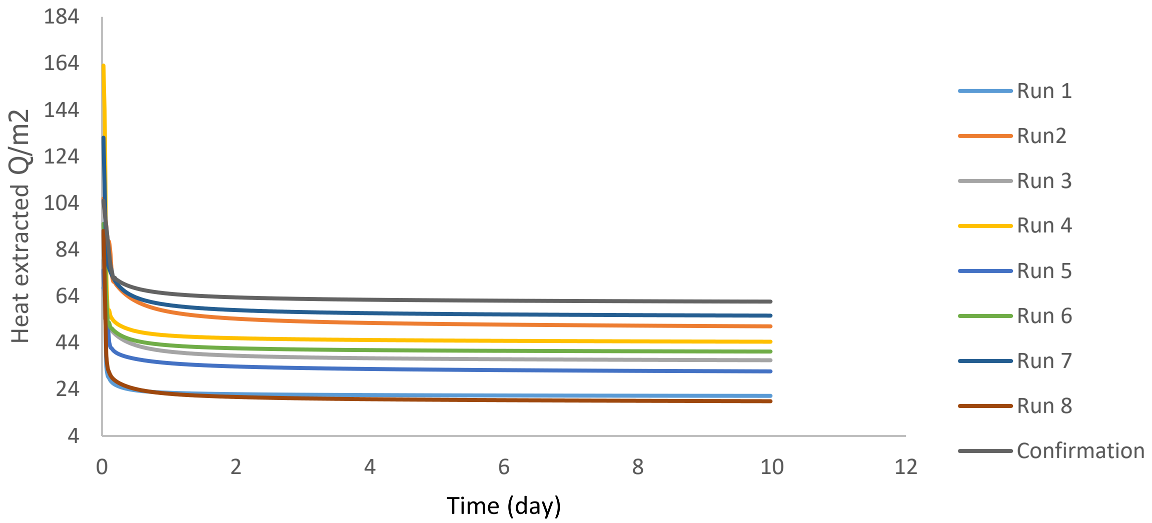

Fig. 7. The heat extracted after 10 days

6.1. Overall analysis of results

The obtained results show that concrete diffusivity and the total pipe length are the most dominant parameters in maximising the thermal output, this observation agrees with previous studies on other types of GHE (e.g. [6], [10]). In terms of the length of pipe, it shows the importance of getting the most out of the available area for heat exchange in order to improve thermal output. Concerning the position of the pipe, as mentioned in the previous section, since the location of the pipe does not affect the concrete cover, positioning the pipe closer to the inside of the tunnel should always be considered.

The pipe thickness used in GHE are very small relative to the size of concrete lining and the soil, hence an increase in the pipe's thermal conductivity is unlikely to yield a quantifiable thermal effect. This is reflected by low the position of pipe's thermal conductivity in the ranking. Pipe spacing and fluid diffusivity were ranked at the bottom of the list, implying that both thermal interferences between pipes and the use of conductivity-enhanced nanofluids play a relatively marginal role in promoting thermal efficiency in energy tunnels. It should be also noted that, due to the statistical nature of the results, only about half of the parameters in the ranking can be considered to have a significant effect [46], hence it does not appear useful to discuss in detail the effect of the last three parameters in the ranking. However, it is worth mentioning that with regards to the use of nanofluids to replace water as the absorber fluid, fluid diffusivity came out 6th on the result table **(Table 11).** This result may be because nanofluids have higher thermal conductivity **(Table 5)** resulting in a higher heat transfer coefficient relative to water. On the other hand, the specific heat of nanofluids is lower compared to water resulting in lower heat transferred.

6.2. Further analysis of dominant parameters

After the influential factors were identified, additional simulations were carried out to further investigate the effect of the dominant parameters on the thermal output, with the exception of concrete diffusivity. Although concrete diffusivity as a parameter is very influential, there is still a lack of intensive research on the possibility of changing the thermal properties of tunnel concrete linings. It is important that the strength of the concrete lining is not compromised by changing its thermal properties (e.g. by selecting/avoiding certain admixtures), as its primary function is structural. Besides, the level of difficulty in achieving improved concrete diffusivity is higher compared to other dominant parameters. Results of the additional simulations are discussed below.

6.2.1. Concrete cover

Considering the effect of concrete cover, additional simulations were run varying the position of the pipes inside the tunnel lining, while keeping the optimal values of the other parameters. The effect was illustrated by plotting the average heat extracted in 10 days (**Fig. 8)**. The heat extracted drops as the absorber pipes are moved further away from the tunnel intrados. The rate of drop is approximately 8% for every 10 cm away from the tunnel inner surface. This observation shows why the position of the pipes was ranked amongst the top three most influential parameters, hence it is important to position the pipes as close as practically possible to the tunnel intrados.

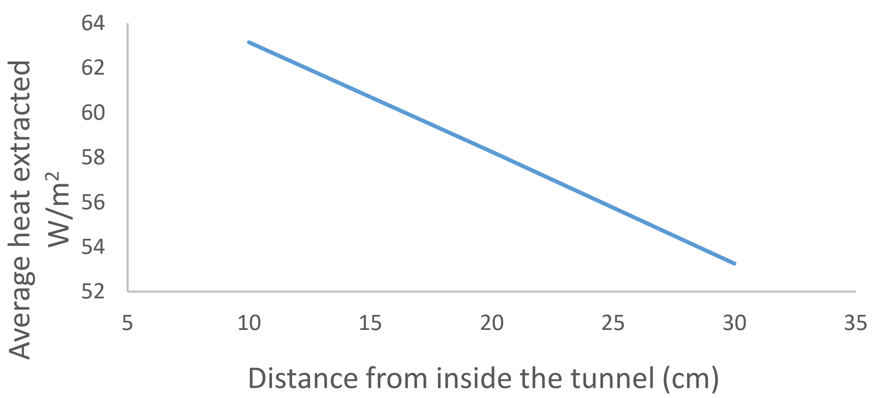

Fig. 8. Effect of pipe location on the heat extraction rate

6.2.2. The total length of pipe

The effect of pipe length was further explored by plotting the fluid temperature change along the length of the pipe during the simulation runs described in Section 5. **Fig. 9** shows the steady-state fluid temperature change along the pipe after 10 days for all the runs. It can be observed that the fluid temperature approaches the soil temperature as the length of the pipes increases, i.e. the outlet temperature is proportional to the length of the pipe, explaining why the total length of the absorber pipe came out as one of the most influential parameters.

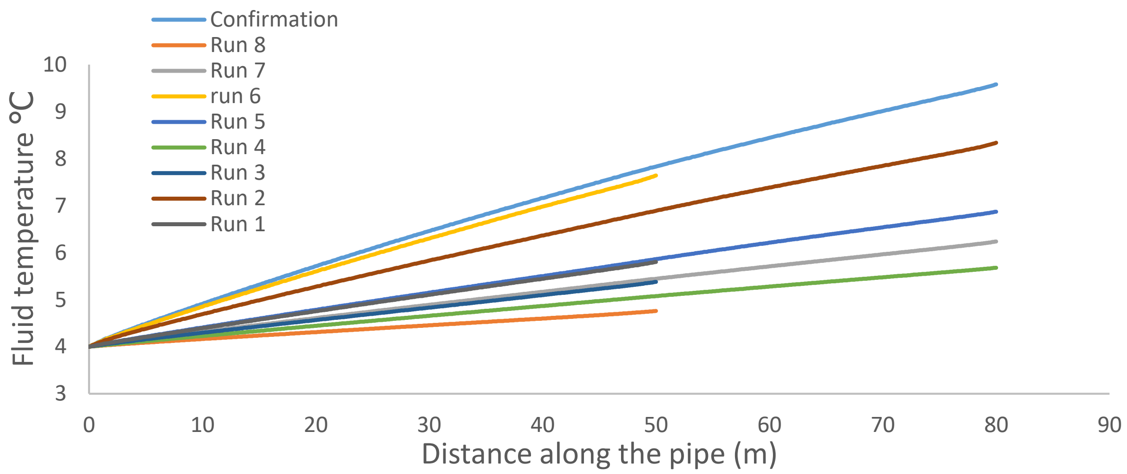

Fig. 9. Fluid temperature variation along the pipe after 10 days.

6.2.3. Pipe diameter

The effect of changing the pipe diameter on the thermal output was analysed together with the corresponding pressure drop required to maintain the flow, which determines the pump power requirements. To analyse these effects, the pipe size and mass flow rate were varied and the result is illustrated and explained below. The pressure drop can be calculated in a simplified manner with a reasonable level of confidence from Moody friction dimensionless parameter f in **Eq. (9)** which has shown to give reasonably accurate results [38].

$$f \equiv \frac{-\left(\frac{dp}{dx}\right) D_{in}}{\rho {u_m}^2/2} \tag{9}$$

Where $\frac{dp}{dx}$ the pressure is gradient, u_m is the average fluid velocity and ρ is the fluid density. The pressure drop is thus derived as:

$$\Delta p = f\frac{\rho {u_m}^2}{2D_{in}}(x_2 - x_1) = f\frac{\rho {u_m}^2}{2D_{in}}L \tag{10}$$

Where *L* is pipes length and x_2, x_1 are the axial positions of the fluid. The pump power required is thus calculated as:

$$P = (\Delta p)\dot{v} \tag{11}$$

where $\dot{v}$ is the volumetric flow rate.

For the range of pipe diameters considered, as expected, at a fixed mass flow rate the pressure drop reduces with increase in pipe diameter. Also, pressure drop increases with increasing mass flow rate for a fixed diameter due to the increase in velocity. Consequently, for a fixed mass flow rate the pump power is inversely proportional to the pipe diameter but increases with an increase in mass flow rate when the diameter is fixed **(Fig. 10)**.

The convective heat transfer coefficient depends on the boundary layer effect in the pipe due to the pipe surface geometry, fluid motion and other properties [38]. **Fig. 11** shows that the heat transfer coefficient in the pipe increases with an increase in mass flow rate at a fixed diameter as a consequence of an increase in the Nusselt number. **Fig. 11** also shows the calculated equivalent heat transfer coefficient which is associated with the total thermal resistance by taking the thermal resistance of the pipe and convection resistance into account. Similarly with increasing mass flow rate, the equivalent heat transfer coefficient increases but not at the same rate as the convective heat transfer coefficient.

Fig. 12 shows that the heat rate increases with an increase in mass flow rate for a fixed diameter due to an increase in the convective heat transfer coefficient. It should be noted that although the average heat rate increases with increasing mass flow rate, the average outlet temperature decreases with an increase in flow rate. This phenomenon could be explained from the fact that at higher flow rate the total time the working fluid spends circulating in the pipe reduces, hence reducing the outlet temperature (i.e., reducing the term $|T_{wO} - T_{wi}|$ in **Eq. 7**).

In summary, heat rate increases with increasing mass flow rate, which leads to an increased pump power requirement. However, it is interesting to note that for a fixed mass flow rate the outlet temperature and hence the heat rate does not vary considerably with increase in diameter. This implies that for a fixed mass flow rate the increase in diameter reduces pressure drop; however, this increase does not result in a significant drop in heat rate. It can be deduced that, in energy tunnels, the use of larger diameter pipes at a fixed mass flow rate to reduce pressure drop does not lead to a significant reduction in thermal output, hence it is more energy-efficient.

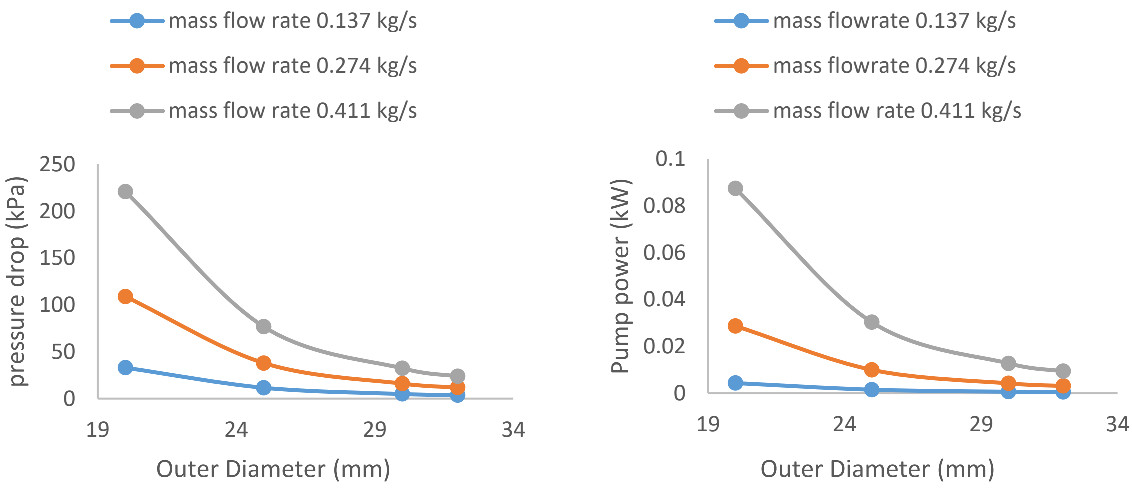

Fig. 10. **a)** **b)**

a) Pressure drop as a function of mass flow rate and pipe diameter

b) Corresponding pump power requirements

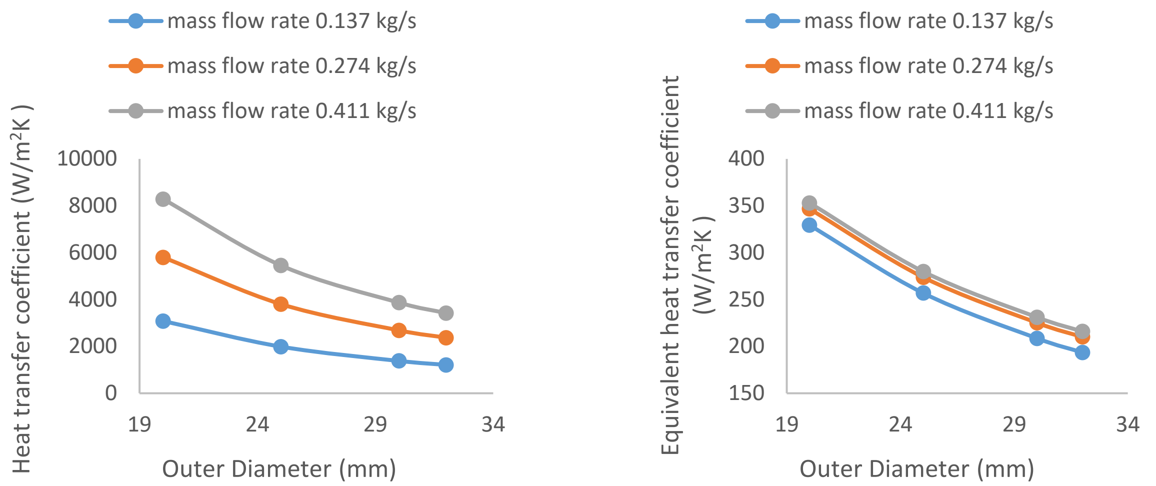

Fig. 11. a) b)

a) Heat transfer coefficient as a function of mass flow rate and pipe diameter

b) Corresponding equivalent heat transfer coefficient

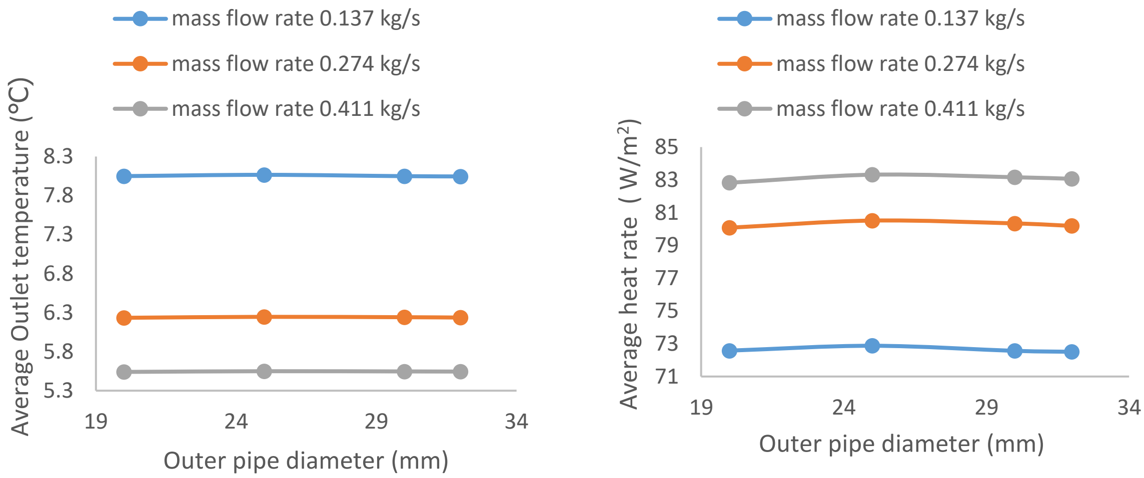

Fig. 12. a) b)

a) Average outlet temperature as a function of mass flow rate and pipe diameter

b) Corresponding Heat rate

7. Conclusion

This paper proposes a comprehensive investigation of the effect of design parameters on the thermal efficiency of an energy tunnel. This was done to provide guidance to practising engineers and researchers dealing with the thermal design of energy tunnels. Seven design parameters were considered, and the Taguchi statistical method was used in order to perform a rational and efficient parametric study. The ranking of parameters from the most to the least influential is as follows: concrete diffusivity, total length, concrete cover and pipe diameter, pipe thermal conductivity, fluid diffusivity and pipe spacing. The main conclusions from this study are highlighted as follows:

- In energy tunnels using concrete aggregate with improved thermal properties is advantageous from a thermal point of view.
- Increasing the total pipe length as much as possible, consistent with the available total heat exchange area is vital in increasing efficiency.
- Positioning the pipes as close to the intrados as practically possible is also very important, especially in hot tunnels, when the energy tunnel is used for space heating.
- When pump power reduction is important, running the heat pump at a lower flow rate should be considered; this can be done by selecting a large pipe diameter since this does not result in a significant loss in thermal output.
- Pipe thermal conductivity does not appear to be influential.
- The absorber fluid thermal diffusivity has little influence. The cost of developing/adopting new nanofluids for use in GSHPs is not justified in energy tunnels, due to a minor impact on the thermal output. In addition to this, nanofluids have relatively high viscosities compared to pure water which would result in a higher pressure drop and more pump power required.
- It is important to control thermal interference between pipes; however, the effect of pipe spacing in energy tunnels is not as pronounced when compared to other GHE installations (like energy piles).
- Further studies could involve extending this approach to account for convection in flowing groundwater, and to investigate the economic effect of enhancing the thermal output of energy tunnels.

References

[1] Wilhelm, J. and L. Rybach, *The geothermal potential of Swiss Alpine tunnels.* Geothermics, 2003. **32**(4-6): p. 557-568.

[2] Mimouni, T., F. Dupray, and S. Minon *Heat Exchanger Anchors for Thermo-active Tunnels* 2013.

[3] Di Donna, A. and M. Barla, *The role of ground conditions on energy tunnels' heat exchange.* Environmental Geotechnics-Journal, 2016. **3**(4): p. 214-224.

[4] Kovačević, M.S., M. Bačić, and I. Arapov, *Possibilities of underground engineering for the use of shallow geothermal energy.* Građevinar, 2012. **64**: p. 1019-1028.

[5] Brandl, H., *Energy foundations and other thermo-active ground structures.* Geotechnique, 2006. **56**(2): p. 81-122.

[6] Cecinato, F. and F.A. Loveridge, *Influences on the thermal efficiency of energy piles.* Energy, 2015. **82**: p. 1021-1033.

[7] Ogunleye, O., et al., *Effect of intermittent operation on the thermal efficiency of energy tunnels under varying tunnel air temperature,.* Renewable Energy, 2019.

[8] Barla, M., A. Di Donna, and A. Perino, *Application of energy tunnels to an urban environment.* Geothermics, 2016. **61**: p. 104-113.

[9] Casasso, A. and R. Sethi, *Efficiency of closed loop geothermal heat pumps: A sensitivity analysis.* Renewable Energy, 2014. **62**: p. 737-746.

[10] Di Donna, A., et al., *Energy performance of diaphragm walls used as heat exchangers.* Proceedings of the Institution of Civil Engineers-Geotechnical Engineering, 2017. **170**(3): p. 232-245.

[11] Loveridge, F. and F. Cecinato, *Thermal performance of thermoactive continuous flight auger piles.* Environmental Geotechnics-Journal, 2016. **3**(4): p. 265-279.

[12] Noorollahi, Y., et al., *The effects of ground heat exchanger parameters changes on geothermal heat pump performance - A review.* Applied Thermal Engineering, 2018. **129**: p. 1645-1658.

[13] Lee, C., et al., *Development of energy textile to use geothermal energy in tunnels.* Tunnelling and Underground Space Technology, 2016. **59**: p. 105-113.

[14] Lee, C., et al., *Evaluation of thermal performance of energy textile installed in Tunnel.* Renewable Energy, 2012. **42**: p. 11-22.

[15] Sani, A.K., et al., *Pipe-pipe thermal interaction in a geothermal energy pile.* Geothermics, 2019. **81**: p. 209-223.

[16] Gordon, D., et al., *Experimental and analytical investigation on pipe sizes for a coaxial borehole heat exchanger.* Renewable Energy, 2018. **115**: p. 946-953.

[17] Raymond, J., S. Mercier, and L. Nguyen, *Designing coaxial ground heat exchangers with a thermally enhanced outer pipe.* Geothermal Energy, 2015. **3**: p. 14.

[18] Bassiouny, R., M.R.O. Ali, and M.K. Hassan, *An idea to enhance the thermal performance of HDPE pipes used for ground-source applications.* Applied Thermal Engineering, 2016. **109**: p. 15-21.

[19] Yoon, S., et al., *Evaluation of stainless steel pipe performance as a ground heat exchanger in ground-source heat-pump system.* Energy, 2016. **113**: p. 328-337.

[20] Raymond, J., et al., *Numerical Modeling of Thermally Enhanced Pipe Performances in Vertical Ground Heat Exchangers.* Ashrae: Transactions 2011, Vol 117, Pt 1, 2011. **117**: p. 899-907.

[21] Park, S., et al., *Constructability and heat exchange efficiency of large diameter cast-in-place energy piles with various configurations of heat exchange pipe.* Applied Thermal Engineering, 2015. **90**: p. 1061-1071.

[22] Nam, Y. and H.B. Chae, *Numerical simulation for the optimum design of ground source heat pump system using building foundation as horizontal heat exchanger.* Energy, 2014. **73**: p. 933-942.
[23] Luo, J., et al., *Thermo-economic analysis of four different types of ground heat exchangers in energy piles.* Applied Thermal Engineering, 2016. **108**: p. 11-19.
[24] Kim, M.J., et al., *Thermal performance evaluation and parametric study of a horizontal ground heat exchanger.* Geothermics, 2016. **60**: p. 134-143.
[25] Kong, X.R., et al., *Experimental and numerical study on the thermal performance of ground source heat pump with a set of designed buried pipes.* Applied Thermal Engineering, 2017. **114**: p. 110-117.
[26] Congedo, P.M., G. Colangelo, and G. Starace, *CFD simulations of horizontal ground heat exchangers: A comparison among different configurations.* Applied Thermal Engineering, 2012. **33-34**: p. 24-32.
[27] Cao, S.J., et al., *Investigation on thermal performance of steel heat exchanger for ground source heat pump systems using full-scale experiments and numerical simulations.* Applied Thermal Engineering, 2017. **115**: p. 91-98.
[28] Dasare, R.R. and S.K. Saha, *Numerical study of horizontal ground heat exchanger for high energy demand applications.* Applied Thermal Engineering, 2015. **85**: p. 252-263.
[29] Zhou, H., J. Lv, and T.L. Li, *Applicability of the pipe structure and flow velocity of vertical ground heat exchanger for ground source heat pump.* Energy and Buildings, 2016. **117**: p. 109-119.
[30] Jun, L., et al., *Evaluation of heat exchange rate of GHE in geothermal heat pump systems.* Renewable Energy, 2009. **34**(12): p. 2898-2904.
[31] Emmi, G., et al., *Energy performance and cost analysis of some borehole heat exchanger configurations with different heat-carrier fluids in mild climates.* Geothermics, 2017. **65**: p. 158-169.
[32] Zhang, W.K., et al., *Investigation on influential factors of engineering design of geothermal heat exchangers.* Applied Thermal Engineering, 2015. **84**: p. 310-319.
[33] Narei, H., R. Ghasempour, and Y. Noorollahi, *The effect of employing nanofluid on reducing the bore length of a vertical ground-source heat pump.* Energy Conversion and Management, 2016. **123**: p. 581-591.
[34] Nataraja, M.C., T.S. Nagaraj, and A. Reddy, *Proportioning concrete mixes with quarry wastes.* Cement Concrete and Aggregates, 2001. **23**(2): p. 81-87.
[35] Zhang, G.Z., et al., *A new model and analytical solution for the heat conduction of tunnel lining ground heat exchangers.* Cold Regions Science and Technology, 2013. **88**: p. 59-66.
[36] Nicholson, D.P., et al., *The design of thermal tunnel energy segments for Crossrail, UK.* Proceedings of the Institution of Civil Engineers-Engineering Sustainability, 2014. **167**(3): p. 118-134.
[37] Fillion, M.H., J. Cote, and J.M. Konrad, *Thermal radiation and conduction properties of materials ranging from sand to rock-fill.* Canadian Geotechnical Journal, 2011. **48**(4): p. 532-542.
[38] Bergman, T.L. and F.P. Incropera, *Fundamentals of heat and mass transfer*. 7th ed. 2011, Hoboken, NJ: Wiley. xxiii, 1048 p.
[39] Choi, J.C., S.R. Lee, and D.S. Lee, *Numerical simulation of vertical ground heat exchangers: Intermittent operation in unsaturated soil conditions.* Computers and Geotechnics, 2011. **38**(8): p. 949-958.
[40] Zhang, L.L., et al., *Analyses on soil temperature responses to intermittent heat rejection from BHEs in soils with groundwater advection.* Energy and Buildings, 2015. **107**: p. 355-365.
[41] Ogunleye, O., *A STUDY ON THE THERMAL PERFORMANCE OF GEOTHERMAL ENERGY TUNNELS* in *Civil Engineering*. 2020, University of Surrey: UK. p. 172.

[42] Guo, L.X., et al., *Thermal Conductivity and Heat Transfer Coefficient of Concrete.* Journal of Wuhan University of Technology-Materials Science Edition, 2011. **26**(4): p. 791-796.

[43] NSAI, *Building components and building elements. Thermal resistance and thermal transmittance - Calculation methods (ISO 6946:2017)*. 2017.

[44] Ghozatloo, A., A. Rashidi, and M. Shariaty-Niassar, *Convective heat transfer enhancement of graphene nanofluids in shell and tube heat exchanger.* Experimental Thermal and Fluid Science, 2014. **53**: p. 136-141.

[45] Cecinato, F. and A. Zervos, *Influence of thermomechanics in the catastrophic collapse of planar landslides.* Canadian Geotechnical Journal, 2012. **49**(2): p. 207-225.

[46] Taguchi, G.U.b.i., E.A. Elsayed, and T.C. Hsiang, *Quality engineering in production systems*. McGraw-Hill series in industrial engineering and management science. 1988, New York: McGraw-Hill. xiv, 173 p.

[47] Peace, G.S., *Taguchi methods : a hands-on approach*. 1993, Reading, Mass.: Addison-Wesley. xxvi, 522 p.

[48] Frodl, S., J.N. Franzius, and T. Bartl *Design and construction of the tunnel geothermal system in Jenbach*. 2010.

[49] Franzius, J.N. and N. Pralle, *Turning segmental tunnels into sources of renewable energy.* Proceedings of the Institution of Civil Engineers-Civil Engineering, 2011. **164**(1): p. 35-40.

[50] Barla, M., A. Di Donna, and A. Insana, *A novel real-scale experimental prototype of energy tunnel.* Tunnelling and Underground Space Technology, 2019. **87**: p. 1-14.

[51] Mimouni, T., F. Dupray, and L. Laloui, *Estimating the geothermal potential of heat-exchanger anchors on a cut-and-cover tunnel.* Geothermics, 2014. **51**: p. 380-387.

[52] Dehdezi, P.K., *Impact of Concrete Thermophysical Properties on Pavement Structural Design.* Journal of Materials in Civil Engineering, 2014. **26**(7): p. 6.

[53] Bucci, A., et al., *Shallow groundwater temperature in the Turin area (NW Italy): vertical distribution and anthropogenic effects.* Environmental Earth Sciences, 2017. **76**(5): p. 14.